Inorg. Chem. **2005**, *44*, 969–978

Cyano-Bridged Structures Based on $[Mn^{II}(N_3O_2\text{-Macrocycle})]^{2+}$: A Synthetic, Structural, and Magnetic Study

Federica Bonadio,[†] Maria-Cristina Senna,[†] JUrgen Ensling,[‡] Andreas Sieber,[†] Antonia Neels,[§] Helen Stoeckli-Evans,[§] and Silvio Decurtins*,[†]

Departement für Chemie und Biochemie, Universität Bern, Freiestrasse 3, CH-3012 Bern, Switzerland, Institut für Anorganische Chemie, Gutenberg Universität Mainz, Staudingerweg 9, D-55099 Mainz, Germany, and Laboratoire de Cristallographie, Institut de Chimie, Université de Neuchâtel, Avenue Bellevaux 51, CH-2007 Neuchâtel, Switzerland

Received June 17, 2004

Reactions between the complex $[Mn^{II}(L)]^{2+}$, where L is a N_3O_2 macrocyclic ligand, and different cyanometalate precursors such as $[M(CN)_n]^{m-}$ (M(III) = Cr, Fe; M(II) = Fe, Ni, Pd, Pt) lead to cyano-bridged molecular assemblies exhibiting a variety of structural topologies. The reaction between $[Mn^{II}(L)]^{2+}$ and $[Fe^{II}(CN)_6]^{4-}$ forms a trinuclear complex with formula $[(Mn^{II}(L)(H_2O))_2(Fe^{II}(\mu\text{-}CN)_2(CN)_4)]\cdot 2MeOH\cdot 10H_2O$ (**1**) which crystallizes in the triclinic space group $P\bar{1}$. The reaction between $[Mn^{II}(L)]^{2+}$ and $[M^{II}(CN)_4]^{2-}$, where M(II) = Ni (**2**), Pd (**3**), Pt (**4**), gives rise to three isostructural linear chain compounds with stoichiometry $[(Mn^{II}(L))(M^{II}(\mu\text{-}CN)_2(CN)_2)]_n$ and which crystallize in the monoclinic space group $C2/c$. The self-assembly between $[Mn^{II}(L)]^{2+}$ with $[M^{III}(CN)_6]^{3-}$, where M(III) = Cr (**5**), Fe (**6**, **7**, **8**), forms three types of compounds. Compounds **5** and **6** are isostructural (monoclinic, space group $P2_1/n$), and the structures comprise anionic linear chains $[(Mn^{II}(L))(M^{III}(\mu\text{-}CN)_2(CN)_4)]_n^{n-}$ with cationic trinuclear complexes $[(Mn^{II}(L)(H_2O))_2(M^{III}(\mu\text{-}CN)_2(CN)_4)]^+$ as counterions. Using an excess of $K_3[Fe^{III}(CN)_6]$, an analogous compound to **6** but with K^+ as counterion is obtained (**7**), which crystallizes in the triclinic space group $P\bar{1}$. Compound **8** consists of 2-D layers with formula $[(Mn^{II}(L))_3(Fe^{III}(\mu\text{-}CN)_4(CN)_2)(Fe^{III}(\mu\text{-}CN)_2(CN)_4)]_n\cdot 2n$MeOH; it crystallizes in the monoclinic space group $P2_1/n$. The magnetic properties were investigated for all samples. In particular, compound **5**, which shows antiferromagnetic exchange interactions between Mn(II) and Cr(III) ions through cyanide bridging ligands, has been studied in detail; the magnetic exchange parameter amounts to $J = -7.5(7)$ cm^{-1}. Compound **8** shows a magnetically ordered phase below 6.4 K which is confirmed by Mössbauer spectroscopy; two hyperfine split spectra were observed below T_c from which $|J|$ values of 2.1 and 1.6 cm^{-1} could be deduced.

Introduction

In recent years, considerable research has been devoted to the design and elaboration of new heterometallic molecular materials with extended structures which have intriguing properties and potential applications in catalysis, electrical conductivity, molecular-based magnetism, and host−guest chemistry.[1,2] A promising approach for this purpose consists of assembling two building blocks that frequently are transition metal complexes, one with terminal ligands able of acting as bridges and another one with available coordination sites. Very popular as a building block is for instance the choice of $[M(CN)_n]^{m-}$ (M = Cr(III), Mn(III), Fe(III), Fe(II)) complexes. Typically, the resulting molecular assemblies often show characteristic multidimensional architectures which may lead to materials exhibiting para-, ferro-, ferri-, or metamagnetism.[3] On the basis of these precursors, many researchers have also focused upon synthesizing discrete cyano-bridged clusters aiming at properties of large total spin ground states preferentially combined with mag-

* To whom correspondence should be addressed. E-mail: silvio.decurtins@iac.unibe.ch.
[†] Universität Bern.
[‡] Gutenberg Universität Mainz.
[§] Université de Neuchâtel.

(1) (a) *Magnetic Molecular Materials*; Gatteschi, D., Kahn, O., Miller, J. S., Palacio, F., Eds.; NATO ASI Series E198; Kluwer Academic Publisher: Dordrecht, The Netherlands, 1991. (b) Kahn, O. *Molecular Magnetism*; VCH: New York, 1993. (c) *Molecular Magnetism: From the molecular Assemblies to the Devices*; Coronado, E., Delhaés, P., Gatteschi, D., Miller, J. S., Eds.; NATO ASI Series E321; Kluwer Academic Publisher: Dordrecht, The Netherlands, 1996.
(2) Lehn, J.-M. *Supramolecular Chemistry, Concepts and Perspectives*; Wiley-VCH, Weinheim, 1995.

10.1021/ic049209u CCC: $30.25
Published on Web 01/20/2005

netic anisotropy,[4] of charge-transfer-induced spin transitions,[5] or of photoinduced high-spin molecules.[6] Furthermore, these $[M(CN)_n]^{m-}$ coordination compounds are also combined with complexes such as $[M^{II}(L)]^{m+}$ (M(II) = Mn, Ni, Cu, and L = diamine or polyamine, or Schiff-base), bearing some labile ligands. In particular, the choice of macrocycles as ligand L has a considerable interest in supramolecular coordination chemistry.[7] For decades, the chemistry of macrocyclic transition metal complexes has seen unprecedent growth, and the trend continues even today. Clearly, on one hand, this chemistry has received continuing impetus from the biochemistry of such macrocycle-containing systems as, for instance, heme proteins. On the other hand, the potential offered to material science by these systems has also been recognized.[8−10] While a substantial body of research on mononuclear macrocyclic compounds has been accomplished, studies in this field are nowadays focused on supramolecular assemblies with varying nuclearities, for example on sequential alignment of metal ion species which are characterized as macrocyclic metal complexes.

For this purpose, the use of macrocycles and chelating ligands in general is a very versatile way to produce materials with largely varied structural properties and functionalities.[11−18]

In 1977, Nelson et al. reported a 15-membered potentially quinquedentate macrocyclic ligand (L) with N_3O_2 donor atoms.[19,20] Thereby, a range of metal ions act as effective templates for the synthesis of pentagonal bipyramidal complexes. Specifically, by a Schiff-base condensation of 2,6-diacetylpyridine and 3,6-dioxaoctane-1,8-diamine in the presence of a manganese(II) salt, the corresponding macrocycle can be isolated as its metal complex. In Chart 1, a drawing of the macrocyclic ligand (L) is shown.

Chart 1

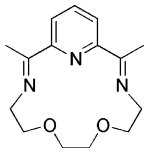

At present, only three structural reports on these specific metal−macrocyclic ligand complexes have been published, and all represent mononuclear species: $[Mn^{II}(L)(NCS)_2]$,[19] $[Mg^{II}(L)(H_2O)_2](ClO_4)_2$,[21] and $[Fe^{II}(L)(CN)_2]\cdot H_2O$.[22] Additionally, the use of lanthanide ions as templates for the formation of this azaoxa-macrocyclic ligand has been investigated, although no structural data based on single crystals have been reported yet.[23,24] The strategy of the present work consists of the self-assembly of the $[Mn^{II}(L)Cl_2]$ unit (L = azaoxamacrocycle: $C_{15}H_{21}N_3O_2$) and $A_3[M^{III}(CN)_6]$ ($A^+ = K^+$, $[NMe_4]^+$; M(III) = Cr(III), Fe(III)), or $K_4[Fe^{II}(CN)_6]$, or $K_2[M^{II}(CN)_4]$ (M(II) = Ni(II), Pd(II), Pt(II)).

Experimental Section

Synthesis and Crystal Growth. All chemicals and solvents were used as received. All preparations and manipulations were performed under aerobic conditions. $[Mn^{II}(L)Cl_2]$ was prepared as described elsewhere with some modifications.[19] *WARNING*: *Cyanides are extremely toxic and should be handled with caution.*

$[Mn^{II}(L)Cl_2]$. 2,6-Diacetylpyridine (1.63 g, 0.01 mol) in methanol (50 mL) was added to a solution of $MnCl_2\cdot 4H_2O$ (1.98 g, 0.01 mol) in methanol (50 mL). The mixture was kept at 50 °C, and a solution of 3,6-dioxaoctano-1,8 diamine (1.48 g, 0.01 mol) in methanol (50 mL) was added over 15 min with continuous stirring. The product was heated to reflux for 6 h, and after that, the solvent was partially removed. By the addition of diethyl ether, an orange precipitate was formed. The product was isolated by filtration, washed with diethyl ether, and air-dried. Yield: 55.1%. Anal. Calcd for $C_{15}H_{25}N_3O_4MnCl_2$: C, 41.21; H, 5.76; N, 9.61. Found: C, 40.54; H, 5.72; N, 9.13. This stoichiometry corresponds to the air-dried product with 2 H_2O molecules, as it was confirmed by TGA analysis. IR (KBr, cm^{-1}): ν 3405 br (OH); 1646 s (C≡N); 1109−1073 s (C−O−C); 1587 s, 832 m, 654 w (py). MS: *mz* ($MnLCl^+$) 367.05, (MnL^{2+}) 329.04.

$[(Mn^{II}(L)(H_2O))_2(Fe^{II}(\mu\text{-}CN)_2(CN)_4)]\cdot 2MeOH\cdot 10H_2O$ (1). In a test tube, 4 mL of an aqueous solution of $K_4[Fe(CN)_6]\cdot 3H_2O$ (96.6 mg, 0.23 mmol) was carefully layered, first with 10 mL of H_2O, and second with 4 mL of a methanol solution of $[Mn(L)Cl_2]$ (50 mg, 0.115 mmol). Diffusion between the two phases over a period of 3 days afforded orange, rod-shaped single crystals

(3) (a) Miyasaka, H.; Ieda, H.; Matsumoto, N.; Sugiura, K.; Yamashita, M. *Inorg. Chem.* **2003**, *42*, 3509. (b) Toma, L. M.; Delgado, F. S.; Ruiz-Perez, C.; Carrasco, R.; Cano, J.; Lloret, F.; Julve, M. *J. Chem. Soc., Dalton Trans.* **2004**, 2836. (c) Van Langenberg, K.; Hockless, D. C. R.; Moubaraki, B.; Murray, K. S. *Synth. Met.* **2001**, *122*, 573. (d) Bonadio, F.; Gross, M.; Stoeckli-Evans, H.; Decurtins, S. *Inorg. Chem.* **2002**, *41*, 5891.

(4) (a) Choi, H. J.; Sokol, J. J.; Long, J. R. *Inorg. Chem.* **2004**, *43*, 1606. (b) Berlinguette, C. P.; Derek, V.; Canada-Vilalta, C.; Galan-Mascaros, J. R.; Dunbar, K. R. *Angew. Chem., Int. Ed.* **2003**, *42*, 1523. (c) Schelter, E. J.; Prosvirin, A. V.; Reiff, W. M. Dunbar, K. R. *Angew. Chem., Int. Ed.* **2004**, *43*, 4912.

(5) Berlinguette, C. P.; Dragulescu-Andrasi, A.; Sieber, A.; Galan-Mascaros, J. R.; Güdel, H. U.; Achim, C.; Dunbar, K. R. *J. Am. Chem. Soc.* **2004**, *126*, 6222.

(6) Herrera, J. M.; Marvaud, V.; Verdaguer, M.; Marrot, J.; Kalisz, M.; Mathonière, C. *Angew. Chem., Int. Ed.* **2004**, *43*, 5468.

(7) Lindoy, L. F. *The Chemistry of Macrocyclic Ligand Complexes*; Cambridge University Press: Cambridge, 1989.

(8) *Macromolecule-Metal Complexes*; Ciardelli, F., Tsuchida, E., Wöhrle, D., Eds.; Springer: Berlin, 1996.

(9) *Comprehensive Supramolecular Chemistry*; Vögtle, F., Ed.; Elsevier Science Ltd.: Oxford, 1996; Vol. 2.

(10) *Phthalocyanines: Properties and Application*; Lever, A. P. B., Leznoff, C. C., Eds.; VCH Publishers: New York, 1989 (Vol 1); 1993 (Vols. 2 and 3); 1996 (Vol. 4).

(11) Guerriero, P.; Tamburini, S.; Vigato, P. A. *Coord. Chem. Rev.* **1995**, *139*, 17.

(12) Ferlay, S.; Mallah, T.; Vaissermann, J.; Bartolomé, F.; Veillet, P.; Verdaguer, M. *J. Chem. Soc., Chem. Commun.* **1996**, 2481.

(13) McAuley, A.; Subramanian, S. *Coord. Chem. Rev.* **2000**, *200*, 75.

(14) Huang, W.; Gou, S.; Hu, D.; Chantrapromma, S.; Fun, H.-K.; Meng, Q. *Inorg. Chem.* **2001**, *40*, 1712.

(15) Kimura, M.; Hamakawa, T.; Hanabusa, K.; Shirai, H.; Kobayashi, N. *Inorg. Chem.* **2001**, *40*, 4775.

(16) Gross, T.; Chevalier, F.; Lindsey, J. S. *Inorg. Chem.* **2001**, *40*, 4762.

(17) Colacio, E.; Dominguez-Vera, J.; Ghazi, M.; Kivekàs, R.; Lloret, F.; Moreno, J. M.; Stoeckli-Evans, H. *J. Chem. Soc., Chem. Commun.* **1999**, 987.

(18) Marvilliers, A.; Parson, S.; Rivière, E.; Audière, J. P.; Kurmoo, M.; Mallah, T. *Eur. J. Inorg. Chem.* **2001**, 1287.

(19) Drew, M. G. B.; Othman, A. H.; McFall, S. G.; McLlroy, P. D. A.; Nelson, S. M. *J. Chem. Soc., Dalton Trans.* **1977**, 1173.

(20) Nelson, S. M. *Pure Appl. Chem.* **1980**, *52*, 2461.

(21) Othman, A. H.; Ng, S. W. *Acta Crystallogr.* **1995**, *C51*, 1059.

(22) Hayami, S.; Gu, Z.; Einaga, Y.; Kobayasi, Y.; Ishikawa, Y.; Yamada, Y.; Fujishima, A.; Sato, O. *Inorg. Chem.* **2001**, *40*, 3240.

(23) Radecka-Paryzek, W.; Patroniak-Krzyminiewska, V. *Polyhedron* **1995**, *14*, 2059.

(24) Patroniak-Krzyminiewska, V.; Radecka-Paryzek, W. *Collect. Czech. Chem. Commun.* **1998**, *63*, 363.

suitable for X-ray analysis. Yield: 25%. Anal. Calcd for $C_{37}H_{70}N_{12}O_{17}FeMn_2$: C, 39.65; H, 6.29; N, 14.99. Found: C, 39.75; H, 5.96; N, 15.74. This stoichiometry corresponds to the air-dried product of **1** with only 1 MeOH and 10 H_2O molecules, as it was confirmed by TGA analysis. IR(KBr, cm^{-1}): ν (C≡N), 2120, 2046 cm^{-1}.

[(Mn^{II}(L))(M^{II}(μ-CN)$_2$(CN)$_2$)]$_n$ (M^{II} = Ni (2), Pd (3), Pt (4)). All three isostructural compounds were prepared in the same manner. Only the detailed synthesis of compound **4** is described here. Yellow, block-like single crystals (yellow-brown block shaped for **2**, and yellow-brown rod-shaped for **3**) suitable for X-ray analysis were obtained in a test tube by carefully layering a methanol solution of [Mn(L)Cl$_2$] (50 mg, 0.115 mmol) onto an aqueous K_2[Pt(CN)$_4$] (41.51 mg, 0.115 mmol) solution and through a diffusion controlled crystallization over a period of some days. Anal. Calcd for $C_{19}H_{21}N_7O_2MnPt$: C, 36.26; H, 3.36; N, 15.58. Found: C, 36.50; H, 3.41; N, 15.35. IR (KBr, cm^{-1}): ν (C≡N), 2136, 2143 cm^{-1}. Anal. Calcd for $C_{19}H_{21}N_7O_2MnNi$: C, 46.28; H, 4.29; N, 19.88. Found: C, 45.81; H, 4.31; N, 19.76. IR (KBr, cm^{-1}): ν (C≡N), 2125, 2136 cm^{-1}.

***n*[(Mn^{II}(L)(H$_2$O))$_2$(Cr^{III}(μ-CN)$_2$(CN)$_4$)]$^+$[(Mn^{II}(L))(Cr^{III}-(μ-CN)$_2$(CN)$_4$)]$_n^{n-}$·7.5*n*H$_2$O (5).** This compound was prepared by adding 5 mL of a methanol solution of [Mn(L)Cl$_2$] (50 mg, 0.115 mmol), to 5 mL of an aqueous solution of K_3[Cr(CN)$_6$] ·2H_2O (79.51 mg, 0.23 mmol). Immediately, a yellow precipitate was formed, and after 30 min of continuous stirring, it was filtered off. Rod-shaped, yellow crystals suitable for X-ray crystal analysis were obtained by slow evaporation of the filtrate over the period of two weeks. Yield: 10%. Anal. Calcd for $C_{57}H_{82}N_{21}O_{15.5}Cr_2Mn_3$: C, 43.37; H, 5.23; N, 18.63. Found: C, 43.47; H, 5.19; N, 18.19. IR(KBr, cm^{-1}): ν (C≡N), 2128, 2147 cm^{-1}.

***n*[(Mn^{II}(L)(H$_2$O))$_2$(Fe^{III}(μ-CN)$_2$(CN)$_4$)]$^+$[(Mn^{II}(L))(Fe^{III}-(μ-CN)$_2$(CN)$_4$)]$_n^{n-}$·8.5*n*H$_2$O (6).** An H-tube was charged with a methanol solution of [Mn(L)Cl$_2$] (50 mg, 0.115 mmol) in one side and an aqueous solution of K_3[Fe(CN)$_6$] (24.9 mg, 0.076 mmol) in the other side. Slow diffusion of the two solutions provides, after some days, brown, rod-shaped single crystals suitable for X-ray analysis. Yield: 35%. Anal. Calcd for $C_{57}H_{84}N_{21}O_{16.5}Fe_2Mn_3$: C, 42.64; H, 5.28; N, 18.34. Found: C, 43.12; H, 5.12; N, 18.49. IR(KBr, cm^{-1}): ν (C≡N), 2075, 2117 and 2130 cm^{-1}.

In addition, the analogous compound containing K^+ as counterion, instead of trinuclear units, has been prepared using an excess of K_3[Fe(CN)$_6$]. The compound has been characterized by single crystal X-ray analysis (**7**).

[(Mn^{II}(L))$_3$(Fe^{III}(μ-CN)$_4$(CN)$_2$)(Fe^{III}(μ-CN)$_2$(CN)$_4$)]$_n$·2*n*MeOH (8). An H-tube was charged with a methanol solution of [Mn(L)Cl$_2$] (100 mg, 0.23 mmol) in one side and a methanol/acetonitrile solution (1:1) of [NMe$_4$]$_3$[Fe(CN)$_6$] (66.6 mg, 0.153 mmol) in the other side. Slow diffusion of the two solutions provides brown, rod-shaped single crystals suitable for X-ray analysis. Yield: 25%. Anal. Calcd for $C_{59}H_{81}N_{21}O_{13}Fe_2Mn_3$: C, 45.17; H, 5.20; N, 18.74. Found: C, 43.35; H, 4.96; N, 18.50. This stoichiometry is confirmed by TGA analysis. IR(KBr, cm^{-1}): ν (C≡N), 2027, 2117 cm^{-1}.

X-ray Crystallography. Intensity data were collected at 153 K on a Stoe Mark II-Image Plate Diffraction System[25] (for **1**, **5**, **6**, **7**) using Mo Kα graphite monochromated radiation. Image plate distances vary from 100 to 130 mm, ω oscillation scans 0−180° at ϕ 0°, and ω oscillation scans 0−180° at ϕ 83° for **1**, 0−18° at ϕ 90° for **5**, 0−44° at ϕ 90° for **6**, 0−60° at ϕ 90° for **7**, step $\Delta\omega$ = 1.0° for **1** and **5**; $\Delta\omega$ = 1.2° for **6** and **7**; 2θ range 2.29−59.53° for **1**, **6**, **7**, 2.50−52.30° for **5**; $d_{max} - d_{min}$ = 17.799−0.716 Å for **1** and **7**, 16.347−0.806 Å for **5**, 16.323−0.772 Å for **6**. For compounds **2**, **4**, and **8**, intensity data were collected at 153 K, for **3** at 293 K, on a Stoe Image Plate Diffraction System[26] using Mo Kα graphite monochromated radiation. Image plate distance of 70 mm, ϕ oscillation scans 0−200°, step $\Delta\phi$ = 1.0°, 2θ range 3.27−52.1° for, $d_{max} - d_{min}$ = 12.45−0.81 Å.

Table 1. Crystallographic Data for [(Mn^{II}LH$_2$O)$_2$(Fe^{II}(μ-CN)$_2$(CN)$_4$)]·2MeOH·10H$_2$O (**1**), [(Mn^{II}L)(Ni^{II}(μ-CN)$_2$(CN)$_2$)]$_n$ (**2**), [(Mn^{II}L)(Pd^{II}(μ-CN)$_2$(CN)$_2$)]$_n$ (**3**), and [(Mn^{II}L)(Pt^{II}(μ-CN)$_2$(CN)$_2$)]$_n$ (**4**)

	1	**2**	**3**	**4**
formula	$C_{38}H_{74}FeMn_2N_{12}O_{18}$	$C_{19}H_{21}MnN_7NiO_2$	$C_{19}H_{21}MnN_7PdO_2$	$C_{19}H_{21}MnN_7PtO_2$
fw,[a] g/mol	1152.82	493.08	540.77	629.46
cryst syst	triclinic	monoclinic	monoclinic	monoclinic
space group	$P\bar{1}$	$C2/c$	$C2/c$	$C2/c$
a, Å	10.6550(11)	17.7973(17)	17.7871(14)	18.0503(18)
b, Å	11.0705(13)	12.0677(12)	11.7403(8)	12.2689(8)
c, Å	11.8646(13)	9.6736(9)	10.6354(9)	9.4884(10)
α, deg	103.606(9)	90	90	90
β, deg	101.826(8)	90.408(11)	90.715(10)	92.496(12)
γ, deg	100.100(9)	90	90	90
V, Å^3	1294.1(2)	2077.6(3)	2220.8(3)	2099.3(3)
Z	1	4	4	4
cryst dimens, mm^3	0.37 × 0.10 × 0.07	0.27 × 0.20 × 0.20	0.50 × 0.22 × 0.20	0.50 × 0.45 × 0.30
T (K)	153(2)	153(2)	293(2)	153(2)
radiation λ,[b] Å	0.71073	0.71073	0.71073	0.71073
ρ_{calcd}, g cm^{-3}	1.479	1.576	1.617	1.992
μ, mm^{-1}	0.837	1.545	1.407	7.289
R[c] [$I > 2\sigma(I)$]	0.0568	0.0362	0.0245	0.0459
wR2[d] [$I > 2\sigma(I)$]	0.1223	0.0799	0.0651	0.1209
GOF[e]	0.959	0.857	1.068	1.016

[a] Including solvent molecules. [b] Graphite monochromated radiation. [c] $R = \sum(||F_o| - |F_c||)/\sum|F_o|$. [d] wR2 = $[\sum(w(|F_o|^2 - |F_c|^2)^2)/\sum(w|F_o|^4)]^{1/2}$. [e] GOF = $[\sum w(|F_o|^2 - |F_c|^2)^2]/(n - p)^{1/2}$, where n is the number of reflections, and p is the number of the refined parameters.

The structures were solved by direct methods using the program SHELXS-97.[27] The refinement and all further calculations were carried out using SHELXL-97.[28] The H-atoms were included in calculated positions and treated as riding atoms using SHELXL default parameters. The non-H atoms were refined anisotropically, using weighted full-matrix least-squares on F^2. Crystallographic data are summarized in Tables 1 and 2. For compound **5**, the crystal was a twin and diffracted weakly beyond 35° in 2θ. For compound **8**, the crystal diffracted poorly, and only ca. 25% of the data can be considered to be observed [$I > 2\sigma(I)$]. The Mn and Fe atoms were refined anisotropically, but the O, N, and C atoms were refined isotropcially, using weighted full-matrix least-squares on F^2.

The macrocycles involving atoms Mn(2) and Mn(3) suffer from considerable thermal motion, resulting in large distortions of the bond distances and angles. The macrocycle involving atom Mn(1), however, was normal within experimental error. This entire fragment was used as a rigid body to model the two other macrocycles in the least-squares refinement. One of the Fe(CN)$_6$ groups [involving atom Fe(1)] suffers from considerable positional disorder (occupancies 0.5:0.5 or 0.6:0.4). A certain amount of disordered solvent was also present, and the SQUEEZE routine in PLATON[29] was used to modify the *hkl* file. This solvent was equated to be equal to 2 molecules of methanol per molecular unit

(25) *X-Area V1.17 & X-RED32 V1.04 Software*; Stoe & Cie GmbH: Darmstadt, Germany, 2002.

(26) *IPDS Software*; Stoe & Cie GmbH: Darmstadt, Germany, 2000.

(27) Sheldrick, G. M. SHELXS-97, Program for Crystal Structure Determination. *Acta Crystallogr.* **1990**, *A46*, 467.

(28) Sheldrick, G. M. *SHELXL-97*; Universität Göttingen: Göttingen, Germany, 1999.

(29) Spek, A. L. *J. Appl. Crystallogr.* **2003**, *36*, 7.

Table 2. Crystallographic Data for $[(Mn^{II}L)(Cr^{III}(\mu\text{-}CN)_2(CN)_4)]_n^{n-}$-$n[(Mn^{II}LH_2O)_2(Cr^{III}(\mu\text{-}CN)_2(CN)_4)]^+ \cdot 7.5nH_2O$ (**5**), $[(Mn^{II}L)$-$(Fe^{III}(\mu\text{-}CN)_2(CN)_4)]_n^{n-}n[(Mn^{II}LH_2O)_2(Fe^{III}(\mu\text{-}CN)_2(CN)_4)]^+ \cdot 8.5nH_2O$ (**6**), $K^+{}_n n[(Mn^{II}LH_2O)_2(Fe^{III}(\mu\text{-}CN)_2(CN)_4)]^+ \cdot nCH_3OH \cdot 8.5nH_2O$ (**7**), and $[(Mn^{II}L)_3(Fe^{III}(\mu\text{-}CN)_4(CN)_2)(Fe^{III}(\mu\text{-}CN)_2(CN)_4)]_n \cdot 2n$MeOH (**8**)

	5	**6**	**7**	**8**
formula	$C_{57}H_{82}Cr_2Mn_3N_{21}O_{15.50}$	$C_{57}H_{84}Fe_2Mn_3N_{21}O_{16.50}$	$C_{22}H_{28}FeMnKN_9O_{4.50}$	$C_{59}H_{71}Fe_2Mn_3N_{21}O_8$
fw,[a] g/mol	1578.26	1603.97	640.42	1478.89
cryst syst	monoclinic	monoclinic	triclinic	monoclinic
space group	$P2_1/n$	$P2_1/n$	$P\bar{1}$	$P2_1/n$
a, Å	16.3911(14)	16.3916(9)	10.817(3)	10.2446(6)
b, Å	10.6924(5)	10.5427(3))	11.415(3)	42.944(4)
c, Å	41.291(3)	41.450(2)	11.851(3)	17.1059(12)
α, deg	90	90	98.12(2)	90
β, deg	94.205(7)	95.248(4)	92.61(2)	102.455(7)
γ, deg	90	90	98.10(2)	90
V, Å^3	7217.2(9)	7133.0(6)	1430.8(7)	7348.5(10)
Z	4	4	2	4
cryst dimens, mm^3	0.50 × 0.15 × 0.15	0.47 × 0.20 × 0.15	0.34 × 0.17 × 0.11	0.40 × 0.10 × 0.08
T (K)	153(2)	153(2)	153(2)	153(2)
radiation λ,[b] Å	0.71073	0.71073	0.71073	0.71073
ρ_{calcd}, g cm^{-3}	1.453	1.494	1.487	1.337
μ, mm^{-1}	0.878	0.992	1.140	0.949
R^c [$I > 2\sigma(I)$]	0.0772	0.0456	0.0494	0.1312
wR2[d] [$I > 2\sigma(I)$]	0.1551	0.1140	0.1202	0.3145
GOF[e]	0.819	0.964	1.022	0.860

[a] Including solvent molecules. [b] Graphite monochromated radiation. [c] $R = \sum(||F_o| - |F_c||)/\sum|F_o|$. [d] wR2 = $[\sum(w(|F_o|^2 - |F_c|^2)^2)/\sum(w|F_o|^4)]^{1/2}$. [e] GOF = $[\sum w(|F_o|^2 - |F_c|^2)^2]/(n - p)^{1/2}$, where n is the number of reflections, and p is the number of the refined parameters.

of complex. The large b-axis (b = 42.944(4) Å) also means that overlap of high angle reflections could not be avoided; after omission of overlapped reflections, only 80% of the full Ewald sphere was available.

Physical Measurements. Magnetic susceptibility data (dc mode) of the polycrystalline samples were collected with a Quantum Design SQUID magnetometer (XL5S) equipped with a 50 kG magnet and operating in the temperature range 300−1.8 K. Pascal's constants were used for the diamagnetic corrections for the samples. The infrared spectra were recorded on a Perkin-Elmer Spectrum One FT-IR spectrometer using KBr pellets. Mössbauer data were collected on a constant-acceleration type Mössbauer spectrometer, equipped with a 1024-channel analyzer operating in the time scale mode, and a 25 mCi ^{57}Co/Rh source was employed. The isomer shifts reported are relative to α-Fe at room temperature. Spectra of the sample (thickness of about 5 mg Fe/cm^2) were collected between 293 and 1.9 K, by means of a combined He continuous flow/bath cryostat. The Mössbauer spectra were analyzed using a computer program EFFINO⟩ [SPI2000].[30]

Results and Discussion

Structural Description. Altogether, eight molecular structures are reported, whereby all of them include the Mn(II) macrocyclic complex which exhibits a distinct coordination pattern around the Mn(II) center. Therefore, at the beginning, a structural description of this $[Mn^{II}(L)(CN)_2]$ complex common to all of these compounds will be presented. Figure 1 shows a representative illustration of the $[Mn^{II}(L)(CN)_2]$ unit.

The Mn(II) ion lies in a pentagonal bipyramidal environment, consisting of the N_3O_2 donor set of the macrocycle forming the basal plane and the two nitrogen atoms of the bridging cyanide ligands occupying the apical positions. Heptacoordinated Mn(II) complexes are relatively uncommon in the literature. Only few examples were known until now,[31−36] and they are particularly rare when only one ligand is able to wrap around this metal ion, such as in $[Mn^{II}(pyo_3tren)]^{2+}$,[33] $[Mn^{II}(TPPA)]$,[34] Mn(II) encapsulated by [21]aneN$_7$,[35] and $[Mn^{II}(N,N,N'$-tris(2-pyridylmethyl)-N'-(2-salicylideneethyl)ethane-1,2-diamine)].[36] Taking into account all the $[Mn^{II}(L)(CN)_2]$ complexes which constitute compounds **1**−**8**, their Mn−N and Mn−O bond lengths vary from 2.196(7) to 2.274(18) Å and from 2.263(17) to 2.318(3) Å, respectively.

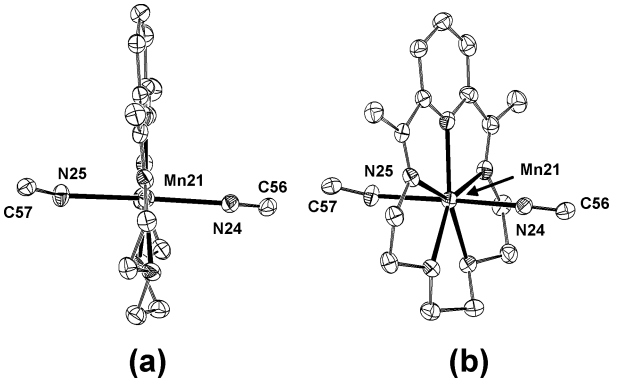

Figure 1. ORTEP representation (ellipsoids at 50% probability) of the molecular structure of the $[Mn^{II}(L)(CN)_2]$ unit of **5**. H atoms are omitted for clarity. (a) Side view. (b) Perspective view.

These distances correspond well with the values found in the mononuclear $[Mn^{II}(L)(NCS)_2]$ complex:[19] Mn−N (av) 2.237 Å and Mn−O (av) 2.283 Å. The angles for **1**−**8** for N−Mn−N vary from 70.4(2)° to 73.4(6)°, for N−Mn−O from 71.0(6)° to 73.6(1)°, and for O−Mn−O from 71.7(2)° to 73.7(1)°. As is shown in Figure 1, the Mn−N−C bonds of the bridging ligands deviate distinctly from linearity, exhibiting an angle of 155.5° (av) at the N-site. In the following, the characteristic structural aspects of the individual eight compounds will be highlighted. Compound **1** crystallizes in the triclinic space group $P\bar{1}$ as a heterometallic assembly with a metal ion stoichiometry Fe(II):Mn(II) = 1:2. The molecular structure consists of a neutral trinuclear compound in which the $[Fe^{II}(CN)_6]^{4-}$ complex is linked by cyanide bridging ligands to two $[Mn^{II}(L)]^{2+}$ units (Figure 2).

Each $[Mn^{II}(L)]^{2+}$ macrocyclic complex possesses two axial ligands, namely one bridging cyanide ligand and one water molecule as a terminal ligand. The central Fe(II) ion, lying on a position with site symmetry C_i, adopts a minimally distorted octahedral coordination geometry. The Fe(II)−C bond length (1.908(3) Å) of the μ-CN$^-$ ligand compares well

(30) [SPI2000]: Spiering, H.; Deak, L.; Bottyan, L. *Hyperfine Interact.* **2000**, *125*, 197.

(31) Tan, X. S.; Xiang, D. F.; Tang, W. X.; Sun, J. *Polyhedron* **1996**, *16*, 689.
(32) Brundenell, S.; Spiccia, L.; Bond, A. M.; Fallon, G. D.; Hockless, D. C. R.; Lazarev, G.; Mahon, P. J.; Tiekink, E. R. T. *Inorg. Chem.* **2000**, *39*, 881.
(33) Gou, S.; You, K.; Yu, K.; Lu, J. *Inorg. Chem.* **1993**, *32*, 1883.
(34) Deroche, A.; Morgenstern-Badarau, I.; Cesario, M.; Guilhem, J.; Keota, B.; Nadjo, L.; Houée-Levin, C. *J. Am. Chem. Soc.* **1996**, *118*, 4567.
(35) Bencini, A.; Bianchi, A.; Dapporto, P.; Garcia-Espana, E.; Marcellino, V.; Micheloni, M.; Paoletti, P.; Paoli, P. *Inorg. Chem.* **1990**, *29*, 1716.
(36) Horner, O.; Girerd, J.-J.; Philouze, C.; Tchertanov, L. *Inorg. Chim. Acta* **1999**, *290*, 139.

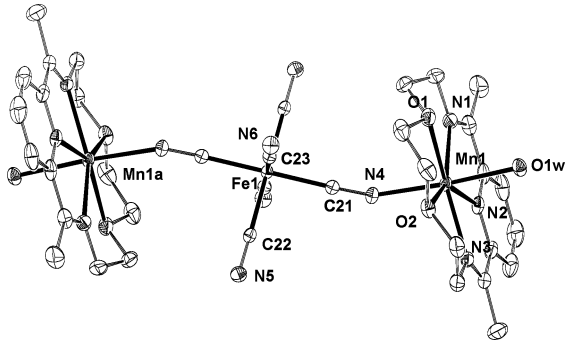

Figure 2. ORTEP representation (ellipsoids at 50% probability) of [(Mn^{II}LH$_2$O)$_2$(Fe^{II}(μ-CN)$_2$(CN)$_4$)]·MeOH·10H$_2$O (**1**). H atoms and solvent molecules are omitted for clarity.

Table 3. Selected Bond Distances (Å) and Bond Angles (deg) for **1**

Mn(1)−N(1)	2.256(3)	Mn(1)−O(2)	2.272(2)
Mn(1)−N(4)	2.171(3)	Mn(1)−O(1w)	2.264(3)
		Fe(1)−C(21)	1.908(3)
N(2)−Mn(1)−N(3)	71.11(11)	N(4)−Mn(1)−(O1w)	174.04(11)
N(3)−Mn(1)−O(2)	73.08(10)	C(21)−Fe(1)−C(22)	91.52(12)
O(2)−Mn(1)−O(1)	72.89(10)	C(21)−Fe(1)−C(23)	89.94(13)

with the literature value (1.923(8) Å) given for the Fe(II)−μ-CN$^-$ system in the Prussian blue phase.[37] Further selected bond lengths and angles are reported in Table 3.

In contrast to the discrete, trinuclear nature of compound **1**, the isostructural compounds **2**, **3**, and **4** form extended cyano-bridged structures. These structures consist of neutral linear chains of alternating [M^{II}(CN)$_4$]$^{2-}$ (M(II) = Ni(II), Pd(II), Pt(II)) and [Mn^{II}(L)]$^{2+}$ complexes, linked by cyanide bridging ligands. As a representative case, a labeled ORTEP plot of compound **4** is shown in Figure 3a.

Each Pt(II) ion occupies a position with site symmetry C_i and is coordinated by two μ-CN$^-$ ligands and two terminal CN$^-$ ligands. Selected bond lengths and angles for **2**, **3**, and **4** are reported in Table 4. The crystal packing of compound **4**, described in the monoclinic space group $C2/c$, is shown in Figure 3b. All interchain distances are longer then 7 Å.

Whereas the above-mentioned compounds turned out to be neutral, the following two isostructural compounds **5** and **6** form ionic species; they crystallize in the monoclinic space group $P2_1/n$. A labeled ORTEP plot of compound **5** is shown in Figure 4. The structure consists of polymeric, anionic chains of alternating cyano-bridged [Cr^{III}(CN)$_6$]$^{3-}$ and [Mn^{II}(L)]$^{2+}$ complexes, and the charge balance is taken over by discrete, cationic trinuclear assemblies [(Mn^{II}(L)(H$_2$O))$_2$-(Cr^{III}(μ-CN)$_2$(CN)$_4$)]$^+$ which contain two water molecules as terminal ligands. Within the chain as well as the discrete trinuclear assemblies, each Cr(III) ion adopts an only minimally distorted octahedral coordination geometry, whereby two cyanide ligands in trans position bridge two [Mn^{II}(L)]$^{2+}$ complexes. The Cr−C−N and Mn−N−C bond angles for bridging cyanide groups are 174.2(7)° (av) and 154.2(6)° (av), respectively. Consequently, the chains deviate from linearity. Selected bond lengths and angles for compounds **5** and **6** are given in Table 5.

Compound **7**, also a charged compound, crystallizes in the triclinic space group $P\bar{1}$ and shows the same linear chain topology of the cyano-bridged complexes as compounds **5**

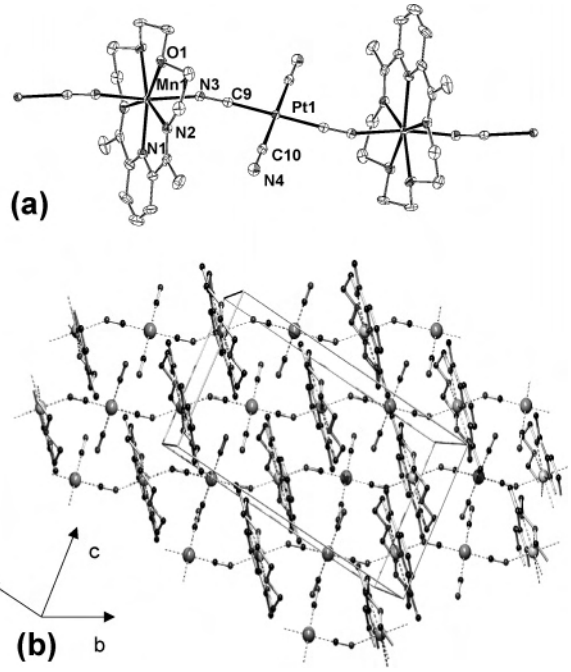

Figure 3. (a) ORTEP representation (ellipsoids at 30% probability) of [(Mn^{II}L)(Pt^{II}(μ-CN)$_2$(CN)$_2$)]$_n$ (**4**). H atoms are omitted for clarity. (b) View of the crystal packing of **4**.

and **6**. However, in this specific case, the cationic trinuclear complexes present in **5** and **6** are now replaced by K$^+$ ions for giving the charge balance to the anionic chains of alternating cyano-bridged [Fe^{III}(CN)$_6$]$^{3-}$ and [Mn^{II}(L)]$^{2+}$ complexes. As shown in Figure 5, the chains are additionally linked by K···N interactions involving two terminal CN$^-$ groups to form a two-dimensional layer structure. In addition, the K$^+$ ions are involved in K···O interactions with methanol molecules with a distances of 2.717(3) Å. Selected bond lengths and angles for **7** are reported in Table 6.

Interestingly, compound **8** displays a neutral two-dimensional structure which is described in the monoclinic space group $P2_1/n$. The extended coordination framework is formed by [Mn^{II}(L)]$^{2+}$, [Fe^{III}(μ-CN)$_4$(CN)$_2$]$^{3-}$, and [Fe^{III}(μ-CN)$_2$(CN)$_4$]$^{3-}$ complexes in a ratio 3:1:1, which are combined to build up a neutral two-dimensional array. A labeled ORTEP plot of the asymmetric unit of compound **8** is shown in Figure 6. The Fe(III) centers display an almost perfect octahedral coordination geometry. The Fe(1) ion is linked by two cyanide bridging ligands to two Mn(II) ions, thereby building up the structure along one dimension, and the four terminal cyanide ligands increase the Fe(1) coordination number to six. The Fe(2) ion is linked by four cyanide bridging ligands to four Mn(II) ions giving rise in this way to a two-dimensional array, and two terminal cyanide ligands complete the Fe(2) coordination sphere. Selected bond lengths and angles for **8** are reported in Table 7. A view of the 2-D crystal packing is shown in Figure 7a; the interlayer arrangement is displayed in Figure 7b.

Magnetic Properties. For compound **1**, the discrete trinuclear assembly, the temperature dependence of the $\chi_M T$

(37) Buser H. J.; Schwarzenbach, D.; Petter, W.; Ludi, A. *Inorg. Chem.* **1977**, *16*, 2704.

Table 4. Selected Bond Distances (Å) and Bond Angles (deg) for **2**, **3**, and **4**

2		**3**		**4**	
Mn(1)−N(1)	2.223(3)	Mn(1)−N(1)	2.210(3)	Mn(1)−N(1)	2.226(6)
Mn(1)−N(3)	2.228(3)	Mn(1)−N(3)	2.227(2)	Mn(1)−N(3)	2.233(5)
Mn(1)−O(1)	2.274(2)	Mn(1)−O(1)	2.263(2)	Mn(1)−O(1)	2.273(5)
Ni(1)−C(9)	1.857(3)	Pd(1)−C(9)	1.977(3)	Pt(1)−C(9)	1.986(7)
N(1)−Mn(1)−N(2)	70.84(6)	N(1)−Mn(1)−N(2)	71.12(5)	N(1)−Mn(1)−N(2)	70.51(16)
N(2)−Mn(1)−O(1)	72.48(8)	N(2)−Mn(1)−O(1)	72.32(7)	N(2)−Mn(1)−O(1)	72.9(2)
C(9)−Ni(1)−C(10)	91.09(14)	C(9)−Pd(1)−C(10)	90.61(11)	C(9)−Pt(1)−C(10)	88.2(2)

Table 5. Selected Bond Distances (Å) and Bond Angles (deg) for **5** and **6**

5		**6**	
Mn(1)−N(1)	2.253(6)	Mn(1)−N(1)	2.245(2)
Mn(1)−N(4)	2.211(7)	Mn(1)−N(4)	2.206(2)
Mn(1)−O(1)	2.280(5)	Mn(1)−O(1)	2.273(2)
Mn(1)−O(1w)	2.186(5)	Mn(1)−O(1w)	2.196(2)
Cr(1)−C(17)	2.052(8)	Fe(1)−C(17)	1.920(3)
Cr(2)−C(56)	2.070(9)	Fe(2)−C(56)	1.952(3)
Mn(21)−N(22)	2.193(7)	Mn(21)−N(22)	2.207(3)
Mn(21)−O(11)	2.271(5)	Mn(21)−O(11)	2.269(2)
N(1)−Mn(1)−N(2)	70.4(2)	N(1)−Mn(1)−(2)	70.65(9)
N(1)−Mn−O(1)	71.7(2)	N(1)−Mn−O(1)	73.59(9)
O(1)−Mn(1)−O(1a)	72.83(19)	O(1)−Mn(1)−O(1a)	72.55(7)
N(4)−Mn(1)−(O1w)	172.6(2)	N(4)−Mn(1)−(O1w)	172.03(10)
C(17)−Cr(1)−C(19)	88.2(3)	C(17)−Fe(1)−C(19)	87.62(12)
C(17)−Cr(1)−C(16)	174.0(3)	C(17)−Fe(1)−C(16)	176.37(12)
N(22)−Mn(21)−N(21)	70.8(2)	N(22)−Mn(21)−N(21)	71.32(9)
N(21)−Mn(21)−O(11)	72.9(2)	N(21)−Mn(21)−O(11)	76.66(9)
N(24)−Mn(21)−N(25)	176.4(2)	N(24)−Mn(21)−N(25)	175.15(9)
C(60)−Cr(2)−C(56)	90.1(3)	C(60)−Fe(2)−C(56)	90.29(12)

Table 6. Selected Bond Distances (Å) and Bond Angles (deg) for **7**

Mn(1)−N(1)	2.252(3)	K(1)−O(30)#5[a]	2.717(3)
Mn(1)−N(4)	2.219(2)	K(1)−N(9)#3	2.733(3)
Mn(1)−O(1)	2.315(2)	K(1)−O(1w)#3	3.044(12)
Fe(1)−C(17)	1.933(3)		
N(1)−Mn(1)−N(2)	70.58(9)	O(30)#5−K(1)−N(9)#3	87.15(10)
N(1)−Mn−O(2)	73.35(9)	O(2wa)−K(1)−N(9)#3	130.0(2)
O(1)−Mn(1)−O(2)	72.78(8)		
C(21)−Fe(1)−C(17)	89.78(11)		

[a] Symmetry transformations used to generate equivalent atoms: #3 $-x$, $-y$, $-z$; #5 x, $y-1$, $z-1$.

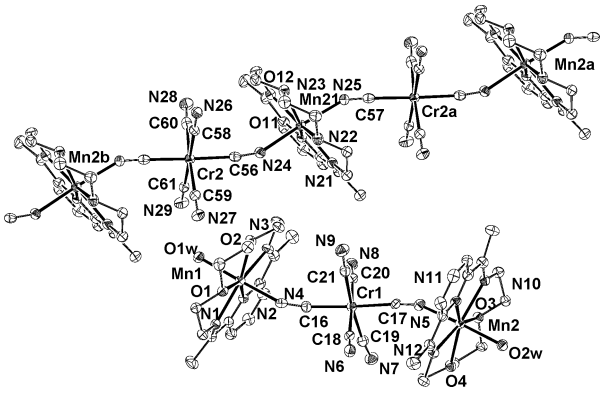

Figure 4. ORTEP representation (ellipsoids at 50% probability) of $n[(Mn^{II}LH_2O)_2(Cr^{III}(\mu\text{-}CN)_2(CN)_4)]^+[(Mn^{II}L)(Cr^{III}(\mu\text{-}CN)_2(CN)_4)]_n^{n-}\cdot 7.5nH_2O$ (**5**). H atoms and solvent molecules are omitted for clarity.

product per $[Mn^{II}_2Fe^{III}]$ unit, measured within an applied magnetic field of 1 kG in the temperature range 1.8−300 K, is shown in Figure 8. The experimental value of 9.02 emu K mol^{-1} at 300 K is in good agreement with the calculated value of 8.75 emu K mol^{-1} for the spin-only value of two high-spin Mn(II) ions ($S = {}^5/_2$). Lowering the temperature to about 4.5 K, the compound shows a paramagnetic behavior corresponding to two isolated Mn(II) ions. Below this temperature, the product of $\chi_M T$ increases, reaching 10.32 emu K mol^{-1} at 2 K, suggesting the presence of a very weak ferromagnetic exchange interaction between the two Mn(II) ions which are linked by the cyano-bridged low-spin Fe(II) ion.[38] In order to estimate the exchange

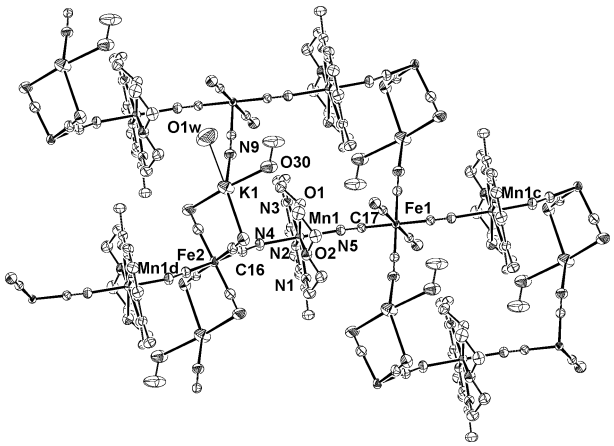

Figure 5. ORTEP representation (ellipsoids at 50% probability) of $nK^+[(Mn^{II}L)(Fe^{III}(\mu\text{-}CN)_2(CN)_4)]_n^{n-}\cdot nCH_3OH\cdot 8.5nH_2O$ (**7**). H atoms and solvent molecules are omitted for clarity.

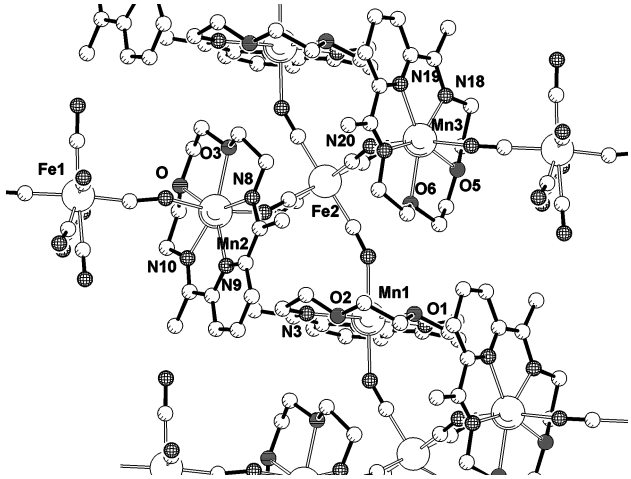

Figure 6. Crystal structure representation emphasizing the asymmetric unit of $[(Mn^{II}L)_3(Fe^{III}(\mu\text{-}CN)_4(CN)_2)(Fe^{III}(\mu\text{-}CN)_2(CN)_4)]_n\cdot 2n$MeOH (**8**). H atoms and solvent molecules are omitted for clarity.

Table 7. Selected Bond Distances (Å) and Bond Angles (deg) for **8**

Mn(1)−N(1)	2.251(16)	N(1)−Mn(1)−N(2)	73.4(6)
Mn(1)−N(4)	2.208(15)	N(1)−Mn−O(1)	71.0(6)
Mn(1)−O(1)	2.308(13)	O(1)−Mn(1)−O(2)	73.3(5)
Fe(1)−C(36)	1.843(18)	C(36)−Fe(1)−C(39)	90.7(9)
Fe(2)−C(20)	1.875(15)	C(57)−Fe(2)−C(18)	89.7(8)

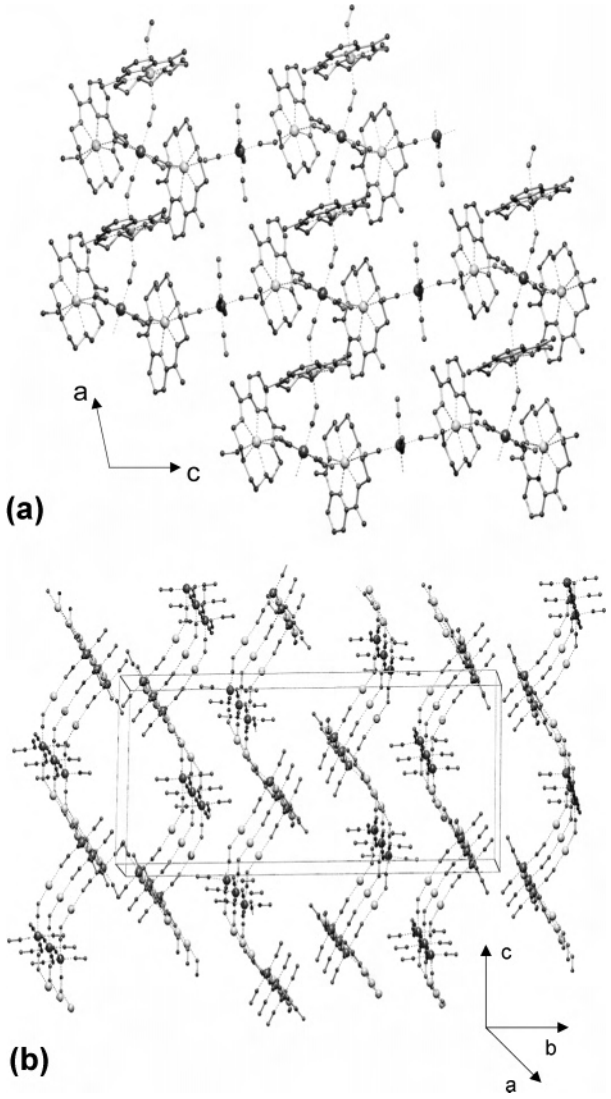

Figure 7. Representation of the crystal packing of compound **8**. H atoms and solvent molecules are omitted for clarity. (a) Projection view in the *ac*-plane. (b) Projection view along the *a*-axis; here, the macrocycles L are omitted for clarity.

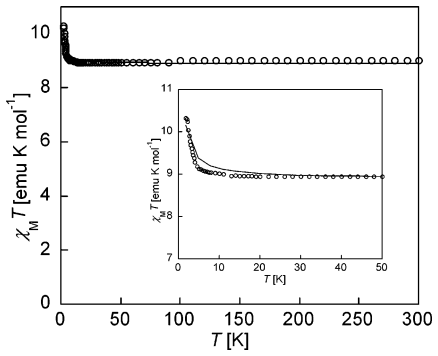

Figure 8. Plot of $\chi_M T$ vs temperature for the polycrystalline compound **1**, measured under a 1 kG magnetic field. The solid line is the best fit obtained with the equation for a Mn(II)−Mn(II) pair.

interaction parameter *J*, the experimental data were fitted on the basis of the isotropic spin-Hamiltonian $H = -2JS_{Mn}S_{Mn}$, for a Mn(II)−Mn(II) pair. The best fit parameters are $J = 0.045$ cm^{-1} and $g = 2.02$, which look very reasonable.

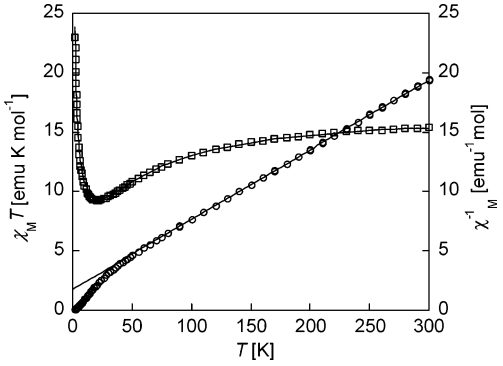

Figure 9. Plot of $\chi_M T$ vs temperature for the polycrystalline compound **5**, measured under a 1 kG magnetic field (□). The solid line is the best calculation obtained with the eq 1. Plot of $1/\chi_M$ vs temperature (○). The solid line is the best fit obtained with a Curie−Weiss law.

Compounds **2**, **3**, and **4** represent the neutral chains where the paramagnetic Mn(II) ions are linked through diamagnetic [M^{II}(μ-CN)$_4$]$^{2-}$ complexes, hence in total a paramagnetic behavior can be expected. To give an example, the $\chi_M T$ product per [Mn^{II}Pt^{II}] unit (compound **4**), measured within an applied magnetic field of 1 kG, gives an experimental value of 4.33 emu K mol^{-1} at 300 K and remains constant while lowering the temperature. The value is in agreement with the calculated value of 4.37 emu K mol^{-1} for the spin-only value of one Mn(II) ion, $S = {}^5/_2$. Definitely, compounds **2** and **3** show the same magnetic behavior.

Compound **5** reveals an interesting case study for a magnetically coupled chain combined with a magnetically interacting trinuclear unit. The temperature dependence of the $\chi_M T$ product per [Cr$^{III}_2$Mn$^{II}_3$] unit, measured within an applied magnetic field of 1 kG in the temperature range 1.8−300 K, is shown in Figure 9.

The experimental value of 15.5 emu K mol^{-1} at 300 K is slightly lower than the calculated value of 16.85 emu K mol^{-1} for the spin-only values of three high-spin Mn(II) ions ($S = {}^5/_2$) and two Cr(III) ions ($S = {}^3/_2$).

On lowering the temperature, $\chi_M T$ versus *T* presents a minimum of 9.28 emu K mol^{-1} at 20 K. The plot of $1/\chi_M$ versus *T* (Figure 9) obeys the Curie−Weiss law (50−300 K) with a Weiss constant $\theta = -30.34$ K, and a Curie constant *C* of 17.04 emu K mol^{-1}. This value is in good agreement with the calculated value of 16.69 emu K mol^{-1} for the spin-only value of three Mn(II) ions, $S = {}^5/_2$, and two Cr(III) ions, $S = {}^3/_2$, assuming $g_{Mn} = g_{Cr} = 2$. The sign of the Weiss constant indicates antiferromagnetic exchange interactions between Mn(II) and Cr(III) ions through the μ-cyano ligands. Below 20 K, $\chi_M T$ versus *T* starts to increase with the further lowering of the temperature, reaching 22.9 emu K mol^{-1} at 2 K. This behavior indicates the presence of ferrimagnetic chains and antiferromagnetically coupled trimers.

In order to obtain a quantitative estimation of the exchange interaction parameter *J*, the experimental data were compared

(38) (a) Buser, H. J.; Ludi, A.; Petter, W.; Schwarzenbach, D. *J. Chem. Soc., Chem. Commun.* **1972**, 1299. (b) Keggin, J. F.; Miles, F. D. *Nature* **1936**, *137*, 577. (c) Ludi, A.; Güdel, H. U. *Struct. Bonding (Berlin)* **1973**, *14*, 1.

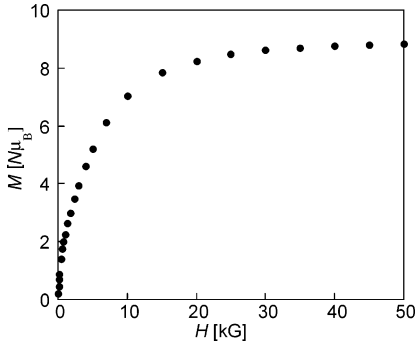

Figure 10. Plot of the field dependence of the magnetization M for the polycrystalline compound **5** at 1.8 K under a magnetic field H up to 50 kG.

with the simulations based on eq 1, which is built up by combining the equation for an antiferromagnetically coupled trimeric Mn(II)−Cr(III)−Mn(II) unit (first summand in eq 1) and a dinuclear Cr(III)−Mn(II) subunit in a ferrimagnetic chain[39] (second summand in eq 1) in a ratio one to one. The spin-Hamiltonian for the trinuclear complex is $H = -2J(S_aS_c + S_bS_c)$. Thus, eq 1 follows as

$$\chi_M T = \frac{N\beta^2}{3k}\left\{ g^2 \sum_{|S_{ab},S\rangle}\left[S(S+1)\frac{(2S+1)e^{-(J/2kT)[S(S+1)-S_{ab}(S_{ab}+1)]}}{\sum_{|S_{ab},S\rangle}(2S+1)e^{-(J/2kT)[S(S+1)-S_{ab}(S_{ab}+1)]}}\right] + 2\left(g^2\frac{1+u}{1-u} + \delta^2\frac{1-u}{1+u}\right)\right\} \quad (1)$$

where S_a and S_b are equal to $^5/_2$ (Mn(II)); S_{ab} is equal to $S_a + S_b$, S is equal to $S_{ab} + S_c$, where S_c is equal to $^3/_2$ (Cr(III)); g^2 is equal to $(g_{a^e} + g_{c^e})/2$, δ^2 is equal to $(g_{a^e} - g_{c^e})/2$, where g_{a^e} is defined as $g[S_a(S_a + 1)]^{1/2}$ and g_{c^e} is defined as $g[S_c(S_c + 1)]^{1/2}$; u is defined as $\coth(J^e/kT) - (kT/J^e)$, where $J^e = J[(S_a(S_a + 1)S_c(S_c + 1)]^{1/2}$. The best-fit parameters are $J = -7.5(7)$ cm^{-1} and $g = 2.00(1)$ (Figure 9).

The field dependence of the magnetization $M/N\mu_B$ measured at 1.8 K under a magnetic field H up to 50 kG (Figure 10) reaches the value of 8.83 $N\mu_B$; that is in good agreement with the expected value of 9 $N\mu_B$ calculated by the sum of the expected ground state spin S for an antiferromagnetically coupled trinuclear complex equal to $2g_{Mn}S_{Mn} - g_{Cr}S_{Cr} = 7\ N\mu_B$ and the expected spin S for a dimeric subunit in the ferrimagnetic chain equal to $g_{Mn}S_{Mn} - g_{Cr}S_{Cr} = 2N\mu_B$.

For the isostructural compound **6**, the temperature dependence of the $\chi_M T$ product per $[Mn^{II}_3Fe^{III}_2]$ unit was measured within an applied magnetic field of 1 kG in the temperature range 1.8−300 K. At room temperature, $\chi_M T$ has a value of 13.95 emu K mol^{-1}, only slightly higher than the spin-only value of 13.85 emu K mol^{-1} calculated for three Mn(II) ions,

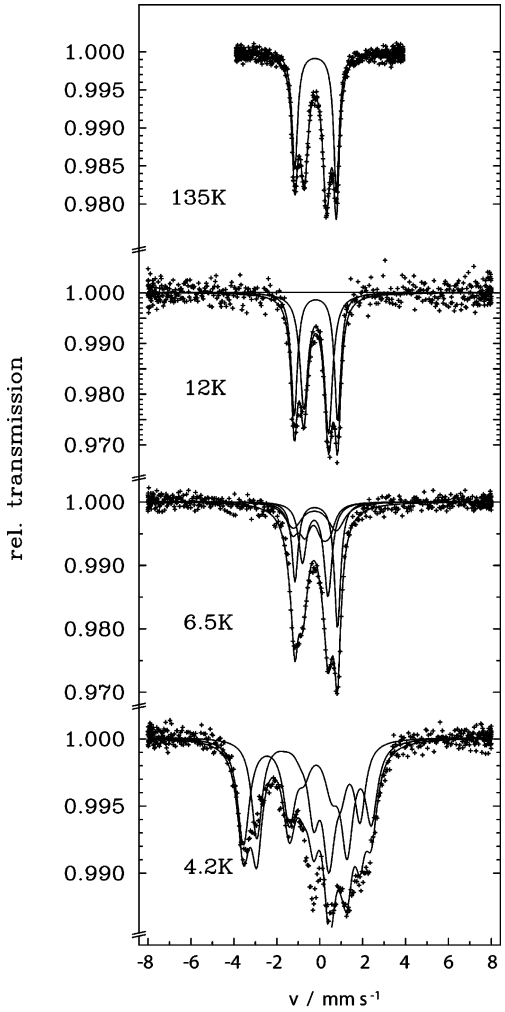

Figure 11. Mössbauer spectra for the polycrystalline compound **8** at different temperatures.

$S = ^5/_2$, and two low-spin Fe(III) ions, $S = 1/2$, assuming $g_{Mn} = g_{Fe} = 2$. On lowering the temperature, $\chi_M T$ versus T increases, suggesting the presence of a ferromagnetic exchange interaction between the Mn(II) and Fe(III) ions through the cyanide bridging ligands. However, the case of a ferromagnetically coupled heterometallic linear chain compound will not be pursued in this report.

For sample **8**, the extended heterometallic Mn(II)/Fe(III) layer compound, the result from a Mössbauer spectroscopy study will be discussed first since this technique reveals a sound data basis for a further elaboration of the magnetic properties. The Mössbauer spectra of a polycrystalline sample at different temperatures are shown in Figure 11.

The room temperature spectrum exhibits two quadrupole doublets with an area ratio of 1:1. Clearly, this reflects the occurrence of two crystallographically independent Fe sites. The isomer shifts (δ(4.2 K) = −0.104 and −0.112 mm s^{-1}) and quadrupole splittings (ΔE_Q = −1.246 and −1.999 mm s^{-1}) are characteristic for low-spin Fe(III) ions.[40] Most importantly, in the 6.5 K spectra, a multiplet structure starts to appear which proves the onset of cooperative magnetic ordering, originating from exchange interactions between the

(39) Drillon, M.; Coronado, E.; Beltran. D.; Georges, R. *Chem. Phys.* **1983**, *79*, 449.

(40) Gütlich, P. In *Mössbauer Spectroscopy*; Topics in Applied Physics, Vol. 5; Springer-Verlag: Berlin, 1985.

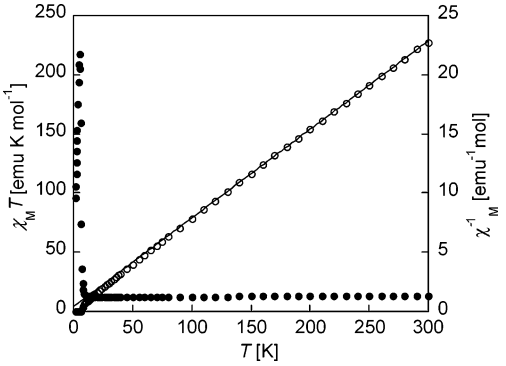

Figure 12. Plot of $\chi_M T$ vs temperature for the polycrystalline compound **8**, measured under a 0.1 kG magnetic field (●). Plot of $1/\chi_M$ vs temperature (○). The solid line is the best fit obtained with a Curie−Weiss law.

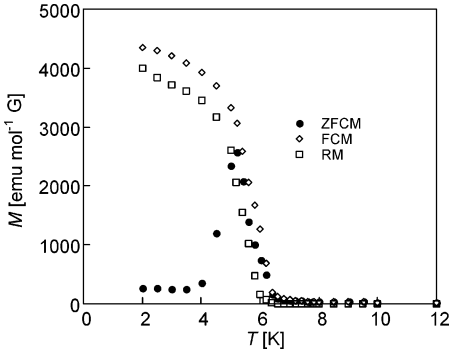

Figure 13. Plot of ZFCM (zero-field-cooled magnetization) (●), FCM (field-cooled magnetization) (◇), in 20 G, RM (remanent magnetization) (□) vs temperature for the polycrystalline compound **8**.

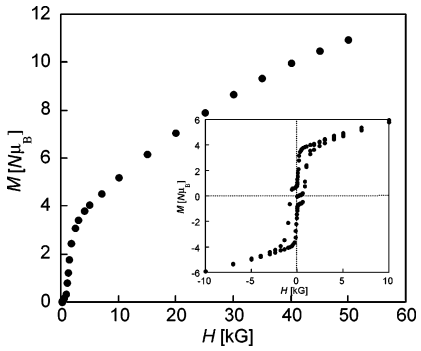

Figure 14. Plot of the field dependences of the magnetization M for the polycrystalline compound **8** at 1.8 K, under a magnetic field H up to 50 kG. The inset shows the hysteresis loop at 1.8 K.

paramagnetic Mn(II) ions ($S = {}^5/_2$) and low-spin Fe(III) ions ($S = {}^1/_2$). Two hyperfine split spectra reveal an internal magnetic field at 4.2 K of 114 and 170 kG each; they are directly deduced from the width of the multiplet pattern. These values lie within the range predicted by the $-220\langle S_z\rangle$ rule for a single unpaired electron. On the basis of a mean-field model, two exchange interaction parameters J can be deduced. Assigning the lower value of the internal field to the [Fe^{III}(μ-CN)$_2$(CN)$_4$)] center and the higher value to the [Fe^{III}(μ-CN)$_4$(CN)$_2$)] center, $|J|$ values of 2.1 and 1.6 cm^{-1} result. These values look reasonable in comparison with the experimental Weiss constant $\theta = -5.7$ K (see below). The magnetic susceptibility data are shown in Figure 12 in form of the temperature dependence of the $\chi_M T$ product per [Mn$^{II}_3$Fe$^{III}_2$] unit, measured within an applied magnetic field of 0.1 kG and in the temperature range 1.8−300 K.

On lowering the temperature, $\chi_M T$ exhibits a minimum of 12.4 emu K mol^{-1} at 30 K, and at temperatures < 10 K, $\chi_M T$ shows an abrupt increase, reaching a maximum of 218 emu K mol^{-1} at 5 K. The plot of $1/\chi_M$ versus T (Figure 12) obeys the Curie−Weiss law in the high temperature region, with a Weiss constant $\theta = -5.7$ K, and a Curie constant C of 13.37 emu K mol^{-1}. This value is in good agreement with the calculated value of 13.87 emu K mol^{-1} for the spin-only value of three Mn(II) ions, $S = {}^5/_2$, and two low-spin Fe(III) ions, $S = {}^1/_2$, assuming $g_{Mn} = g_{Fe} = 2$. The sign of the Weiss constant θ indicates antiferromagnetic exchange interactions between Mn(II) and Fe(III) ions through the μ-CN$^-$ ligands. These observations, in agreement with the Mössbauer data, suggest the onset of a ferrimagnetically ordered phase at temperatures below 7 K. In addition, Figure 13 displays the field-cooled magnetization (FCM), zero-field-cooled magnetization (ZFCM), and remanent magnetization (RM) performed in the temperature range 1.8−12 K. The FCM, obtained by cooling the sample under 20 G, shows a steep increase when the temperature is lowered below 6.5 K.

When the field is switched off at 1.8 K, a remanent magnetization (RM) is observed which vanishes as the temperature is increased to 6.4 K. The ZFCM (cooling in zero field and warming up under 20 G) merges with the FCM curve as the temperature is raised. Overall, these characteristics are in agreement with a magnetically correlated phase with a critical temperature T_c of about 6.4 K. The field-dependent magnetization was measured up to 50 kG at 1.8 K. The curve shows a sigmoidal shape, typical for a metamagnet (Figure 14).

The magnetization first increases slowly with increasing H, confirming the antiferromagnetic interlayer interactions, and then above about 1000 G, it rises steeply due to a flipping from an antiferromagnetic to a ferromagnetic interlayer spin arrangement. The expected saturation value of 13 $N\mu_B$ for 3 $g_{Mn}S_{Mn} - 2g_{Fe}S_{Fe}$ is not yet reached at 50 kG. The magnetization $M/N\mu_B$ versus magnetic field H curve exhibits a hysteresis loop with a remanent magnetization of 1.0 $N\mu_B$ and a coercive field of 1160 G (Figure 14 inset).

This overall magnetic behavior is a signature of a complex magnetic structure, but it is clearly indicating the presence of a net magnetic moment in the 3-D antiferromagnetic phase, which is very probably due to spin canting.

Concluding Comments

The eight compounds described in this paper are the first examples of extended coordination polymers using [Mn^{II}(L)]$^{2+}$ (L = N$_3$O$_2$ macrocyclic ligand) as building block in combination with metallocyanide complexes. They crystallize with different structural topologies: discrete heterometallic assemblies, heterometallic linear chains, and heterometallic 2-D layers. All the compounds possess the same coordination pattern around the Mn(II) centers. Compound **1** exhibits a very small ferromagnetic exchange interaction between the Mn(II) ions mediated through the cyano-bridged

low-spin Fe(II) ion. The linear chain compounds (**2**, **3**, **4**) do not show any noteworthy magnetic properties, which is due to the presence of diamagnetic $[M^{II}(CN)_4]^{2-}$ complexes. The substitution of $[M^{II}(CN)_4]^{2-}$ by $[M^{III}(CN)_6]^{3-}$ leads to anionic linear chains (**5**, **6**, **7**). Compound **5** reveals antiferromagnetic exchange interactions between the Mn(II) and Cr(III) ions through cyanide bridging ligands, and the estimation of the exchange interaction parameter *J* has been evaluated theoretically. Compound **8** shows a different structural topology, namely a 2-D layer system, and the study of the magnetic properties combined with Mössbauer spectroscopy reveals a magnetically ordered phase below 6.5 K. In addition, a metamagnetic behavior is found with a critical field of 1 kG at 1.8 K. It is noteworthy that, at 1.8 K and very low field, this compound exhibits a net magnetic moment, which is most likely due to spin canting.

Acknowledgment. This work was supported by the Swiss National Science Foundation through Project 4047-057532/2. The authors thank Professor Fernando Palacio for helpful discussions.

Supporting Information Available: X-ray crystallographic files in CIF format for compounds **1**−**8**. This material is available free of charge via the Internet at http://pubs.acs.org.

IC049209U